Determination of the Geometry Factor for Longitudinal Perturbations in Space-Charge Dominated Beams

J. G. Wang, H. Suk, D. X. Wang, and M. Reiser
Institute for Plasma Research, University of Maryland, College Park, Maryland 20742
(Received 18 October 1993)

We present the results of an experimental investigation of the parametric dependence of the geometry factor g associated with line-charge perturbations in space-charge dominated beams. The experiment consists of a novel method of launching localized space-charge waves and measuring simultaneously the wave velocity and the radius a of an electron beam propagating through a periodic focusing channel with pipe radius b. We find that the g factor obeys the relation $g=2\ln(b/a)$. This result is supported by theoretical analysis, and is also in agreement with previous theoretical work. The experimental technique can be used for any type of beam, whether space charge dominates over emittance or not.

PACS numbers: 41.85.Ja, 29.27.Bd, 29.27.Fh, 52.35.−g

The geometry factor g is an important parameter in longitudinal beam dynamics, which is discussed in most accelerator and beam physics books [1–5], as well as in other literature on plasma physics and fusion energy research, microwave theory and devices [6–8], etc. It relates the longitudinal electric field associated with a perturbation in a beam with the line-charge density variation. Under the long-wavelength limit this relationship can be expressed in the form

$$E_z(z,t)\cong -\frac{g}{4\pi\varepsilon_0\gamma^2}\frac{\partial\Lambda_1(z,t)}{\partial z}, \tag{1}$$

where $\Lambda_1(z,t)$ is the perturbed line-charge density, ε_0 is the permittivity of free space, and γ is the Lorentz factor. For a round, unbunched beam of radius a in a pipe of radius b the g factor can be represented by the general, long-wavelength formula

$$g=2\ln(b/a)+\alpha, \tag{2}$$

where α is a constant for which different values (1, 0.5, and 0) can be found in the literature. Neil and Sessler, in their original work [9], treated longitudinal instabilities of beams in particle accelerators. They used a uniform-beam model with constant radius a, and derived the relation

$$\alpha=1-(r/a)^2, \tag{3}$$

with r being the radial position within the beam. This relation implies that the g factor, as well as the field E_z, is a maximum with $\alpha=1$ on the axis, and reduces parabolically to a minimum with $\alpha=0$ on the beam edge. Averaging the field over the beam cross section yields $\alpha=0.5$. Hence, there is the question as to which value of α should be used. Indeed, Neil and Sessler raised this question from the very beginning: "This involves some average of E_z over the beam cross section but... the precise average required is not clear. Because E_z varies slowly across the beam, we will... employ E_z $(r=0)$, although E_z $(r=a)$ is probably more accurate." In the literature following this early work most authors (e.g., [3,4]) use the value $\alpha=1$ though the average value of $\alpha=0.5$ would be more appropriate. The constant-radius assumption applies to emittance-dominated beams, as in circular accelerators. However, such beams have a Gaussian profile, and it is not clear to what extent the results of the uniform-beam model are valid. For space-charge dominated beams, the uniformity of the particle density is a good approximation, but the radius does not remain constant so that Eq. (3) is not applicable. These questions concerning the theoretical models have motivated our investigation. So far, to the best of our knowledge, there has been no report on any measurement of the g factor which would permit a direct comparison and check with the theory.

We have developed a novel method to determine, for the first time, the parametric dependence of the g factor associated with longitudinal perturbations in a beam. In this technique, localized space-charge waves are launched on the electron beam in a periodic solenoidal focusing channel and the propagation velocities of these waves are measured. At the same time, the beam radius a is independently measured by a phosphor screen plus charge-coupled device (CCD) camera technique. This leads to an experimental determination of the parametric dependence of the geometry factor g on the radius a. We used this method to determine the g factor in the case of our space-charge dominated electron beam, as will be discussed below.

The experimental setup shown in Fig. 1 consists of an electron beam injector [10] and a 5-m-long periodic solenoidal focusing channel [11]. The key device in the injector is a gridded electron gun which is able to produce the desired beam parameters with localized perturbations [12]. When the beam propagates downstream, the wave speed can be measured accurately by five fast current monitors. Typical beam parameters in the experiment are beam energy of 5 keV, beam current of 50 to 70 mA, transverse effective emittance (4×rms) of about 90 μrad, and pulse length of 70 ns. The localized space-charge waves are positioned on the central region of the beam

0031-9007/94/72(13)/2029(4)$06.00

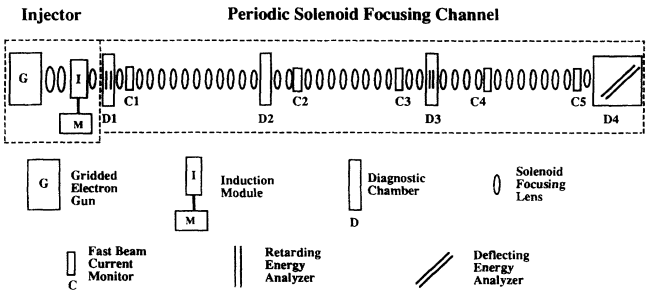

FIG. 1. Schematic of experimental setup.

pulse. The maximum traveling time of the waves is less than 10 ns. Thus, the flat-topped 70 ns beam pulse acts like a continuous beam for the propagation of the space-charge waves, and the nonlinear space-charge forces at the ends of the beam pulse have no effect on the measurement. The solenoidal transport channel consists of 36 periodically spaced lenses, with period length of $S=13.6$ cm. Three additional lenses are used to match the beam from the gun into the channel. The phase advance σ_0 of the particle betatron oscillation per period without space charge, which is a measure of the magnetic focusing strength, is varied between 45° and 90°. With these parameters the phase advance σ of the particle betatron oscillation per period with space charge is in the range of $0.19\sigma_0$ to $0.34\sigma_0$. Such a large tune depression implies that the beam is space-charge dominated so that the uniform beam model for the propagation of space-charge waves is valid.

Figure 2 shows the beam current signals at three different locations along the channel. The beam current in this measurement is 56 mA. It can be seen clearly that the two (slow and fast) space-charge waves move away from each other. The velocity c_s of the space-charge waves in the beam frame is determined by the longitudinal force and is theoretically related to the geometry factor g by

$$c_s=(eg\Lambda_0/4\pi m\varepsilon_0\gamma^5)^{1/2}, \tag{4}$$

where Λ_0 is the unperturbed line-charge density of the beam, and e/m denotes the ratio of charge to mass of the particles. The time interval between the two space-charge waves, which can be measured very accurately at different locations along the channel, is related to the traveling distance z by

$$\Delta t=\frac{2c_s}{v_0^2-c_s^2}z, \tag{5}$$

where v_0 is the beam velocity. Figure 3 plots the time interval of the two space-charge waves as a function of the channel distance for two different phase advances σ_0, where the beam energy is 5 keV and the beam current is about 56 mA in the experiment. A least-squares fitting of the experimental data yields $\Delta t/z$, and hence the wave velocity c_s according to Eq. (5); using this value of c_s one can determine the geometry factor g from Eq. (4).

The beam radius a is measured by the phosphor screen plus CCD camera technique [13]. A typical beam image and its profile are shown in Fig. 4, indicating a relatively flat-topped, uniform density distribution across the beam, which is consistent with a space-charged dominated beam. The diameter of this image is measured by its FWHM (full width at half maximum). Because of the

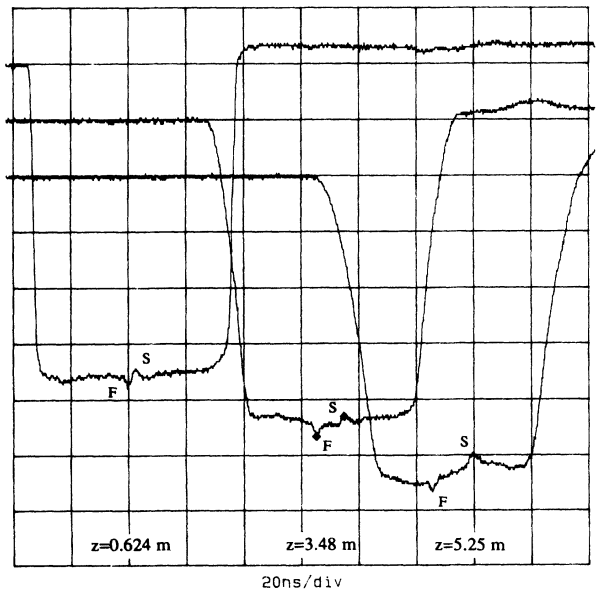

FIG. 2. Beam current wave forms with perturbations measured at the channel distances of $z=0.624$ m, $z=3.48$ m, and $z=5.25$ m, respectively ($z=0$ is the cathode position), where F is for the fast wave and S is for the slow wave (ordinate is the current amplitude in relative scale).

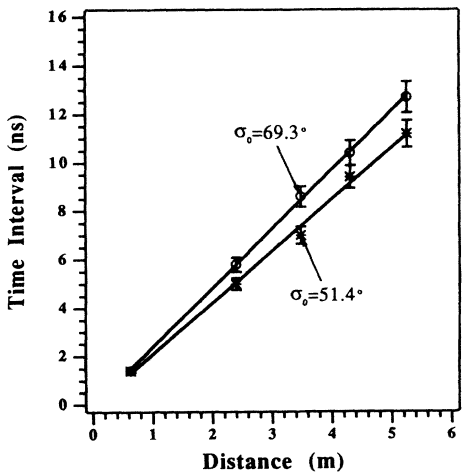

FIG. 3. Time interval between two space-charge waves vs drifting distance for two different phase advances σ_0, as measured by the five current monitors. The solid lines are least-squares fits of the experimental data.

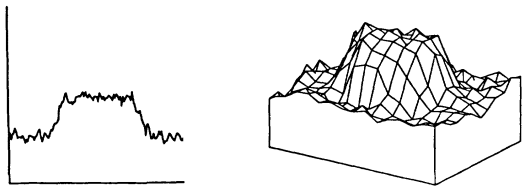

FIG. 4. Typical beam image and its profile, showing a uniform density distribution across the beam.

periodic focusing, the beam performs envelope oscillations under matched conditions. The measured matched beam envelopes in the last two periods of the channel for two different phase advances σ_0 are shown in Fig. 5. The average beam radii are obtained from these experimental data. In the experiment the beam radius a can be changed by adjusting the phase advance σ_0 at a fixed beam energy and current, or by varying the beam energy and current at a fixed phase advance σ_0. In Fig. 6 the measured average beam radii for seven different experimental conditions are compared with the results from the smooth-approximation theory [5], showing a very good agreement between the experiment and theory.

Using the two experimental results for the g factor and the beam radius a, we plotted the g factor against the corresponding beam radius in the form of $\ln(b/a)$ for different experimental conditions as shown in Fig. 7. A least-squares fitting of these data yields the relation of the g factor as a function of the beam radius a, suggesting that the correct formula for the g factor is $g=2\ln(b/a)$, i.e., $\alpha=0$.

The theoretical formulas (1) to (3) for the longitudinal electric field within the beam and the geometry factor g can be derived following the approach in Refs. [9,14]. A schematic is shown in Fig. 8 to depict the procedure. Under the long-wavelength condition, e.g., $\lambda \gg b/\gamma$, where λ is the wavelength of the perturbation, the radial electric field and the azimuthal magnetic field are given approximately by

$$E_r \cong \frac{\Lambda}{2\pi\varepsilon_0}\frac{r}{a^2}, \quad r \le a, \qquad \frac{\Lambda}{2\pi\varepsilon_0}\frac{1}{r}, \quad r \ge a, \tag{6}$$

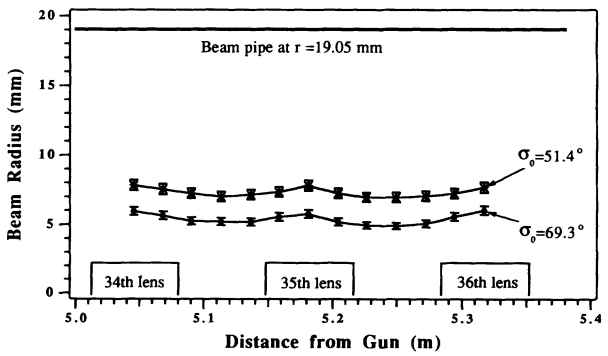

FIG. 5. Measured beam envelope in the last two periods of the channel for two different phase advances σ_0.

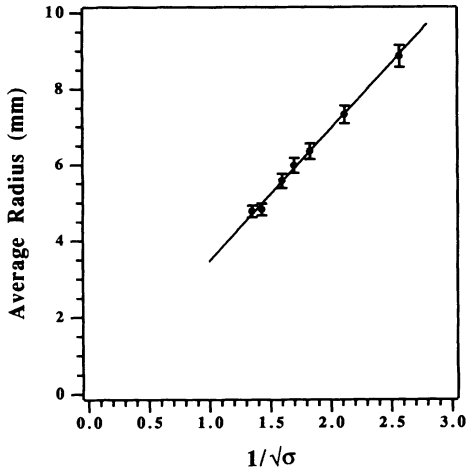

FIG. 6. Comparison between the experimental beam radius (the data points) and the result from the smooth approximation theory (the solid line), where σ is the phase advance with space charge.

$$B_\theta \cong \frac{\Lambda v_0 \mu_0}{2\pi}\frac{r}{a^2}, \quad r \le a, \qquad \frac{\Lambda v_0 \mu_0}{2\pi}\frac{1}{r}, \quad r \ge a, \tag{7}$$

where Λ is the line-charge density of the beam and μ_0 is the permeability of free space. Applying Faraday's law in the dashed rectangular area yields Eqs. (1) to (3). In the derivation, the authors of Refs. [9,14] used a uniform beam model and the following two assumptions: All the perturbed quantities vary as $e^{i(\omega t - kz)}$, including the beam volume density ρ; the beam radius a is constant. If the space-charge forces play a significant role, the assumption of a constant beam radius under perturbations is no longer valid, as mentioned above. To model the average behavior of the beam radius we used the K-V envelope

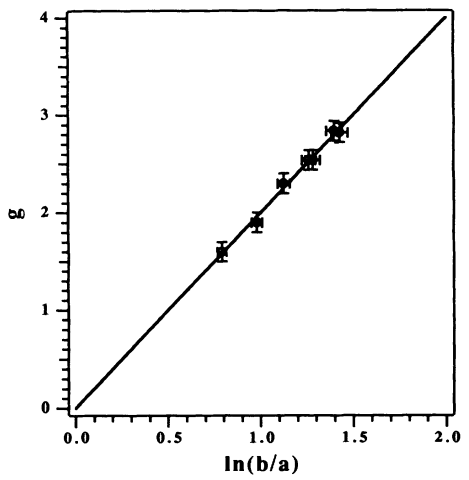

FIG. 7. The measured g factor vs $\ln(b/a)$. A least-squares fitting of the experimental data yields $g \approx 2.01\ln(b/a) - 0.01$, suggesting the correct formula $g=2\ln(b/a)$ as indicated by the solid line.

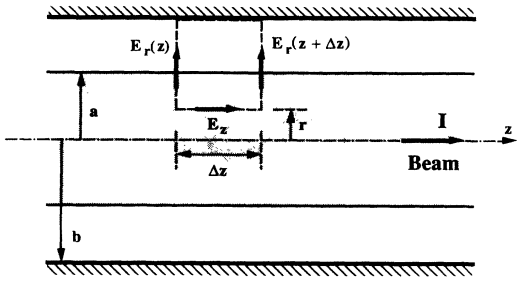

FIG. 8. Configuration to derive theoretical formula for the g factor.

equation for a matched beam in the smooth approximation which yields the approximate relation [5]

$$a(z) \cong \left[\frac{\Lambda(z)}{C} + \frac{\varepsilon}{k_0} \right]^{1/2}, \tag{8}$$

where $C = 2\pi\varepsilon_0 (mc^2/q)\beta^3\gamma^2 k_0^2$, $k_0 = \sigma_0/S$, and ε is the transverse emittance. In an emittance-dominated beam, where $\varepsilon/k_0 \gg \Lambda(z)/C$, perturbations of the line-charge density $\Lambda(z)$ have a negligible effect on the beam radius so that a =const is a good assumption. The perturbation of $\Lambda(z)$ appears as a longitudinal variation of the volume charge density $\rho(z)$ in this case. By contrast, if space charge dominates, we find from (8) that the beam radius changes according to $a^2(z) \approx \Lambda(z)/C$ and hence that the volume charge density ρ remains constant, i.e., independent of z [5],

$$\rho = \frac{\Lambda(z)}{\pi a^2(z)} = \frac{C}{\pi} = \text{const}. \tag{9}$$

Following the approach of Refs. [9,14] but using Eq. (9) instead of a =const, we derived the relation

$$g = 2\ln(b/a) \tag{10}$$

for a space-charge dominated beam. This agrees with our experimental results. For an emittance-dominated beam (a =const) we recover the results (2) and (3) of Neil and Sessler [9] (see Ref. [5] for further details). The relation (10) can also be deduced from previous works based on the field theory approach [15–17] and can be found in Ref. [18], where the method based on fluid equations was employed.

From Eqs. (1) and (10) it follows that the longitudinal electric field E_z inside of the beam is independent of the radial position. The experimental parameters show that the reactive skin depth c/ω_p, where c is the speed of light and ω_p is the plasma frequency, is much larger than the beam radius a. Thus the field E_z in the interior of the beam is not zero, as one might infer from the "surface-wave" concept [17,18], which does not apply to the long-wavelength limit of our model and the experiment. Although the volume density remains unperturbed, we observed experimentally that the velocities of the particles within the beam are perturbed, as well as the beam current.

In conclusion, we have developed a novel method for the experimental determination of the g factor associated with longitudinal charge perturbations in unbunched beams. We also reported the results of a theoretical analysis in which the variation of the beam radius with space charge and emittance is accounted for. The new experimental technique was applied to a space-charge dominated electron beam, and the experimentally determined relation for the g factor was found to be in good agreement with our own analysis and with the results of different previous theoretical models.

The authors would like to acknowledge useful discussions about this problem with J. D. Lawson and I. Haber. This research was supported by the U.S. Department of Energy and ONR.

[1] J. D. Lawson, *The Physics of Charged-Particle Beams* (Oxford Univ. Press, New York, 1988), 2nd ed., Sec. 6.3.
[2] S. Humphries, Jr., *Charged Particle Beams* (Wiley, New York, 1990), Sec. 14.2.
[3] D. A. Edwards and M. J. Syphers, *An Introduction to the Physics of High Energy Accelerators* (Wiley, New York, 1992), Sec. 5.2.
[4] A. W. Chao, *Physics of Collective Beam Instabilities in High Energy Accelerators* (Wiley, New York, 1993), Sec. 1.5.
[5] M. Reiser, "Theory and Design of Charged Particle Beams" (Wiley, New York, to be published), Sec. 6.3.2.
[6] R. B. Miller, *An Introduction to the Physics of Intense Charged Particle Beams* (Plenum, New York, 1982), Sec. 3.3.
[7] R. C. Davidson, *Physics of Nonneutral Plasmas* (Addison-Wesley, New York, 1990), Sec. 5.4, for example.
[8] A. H. W. Beck, *Space-Charge Waves and Slow Electromagnetic Waves* (Pergamon, New York, 1958).
[9] V. K. Neil and A. M. Sessler, Rev. Sci. Instrum. **36**, 429 (1965).
[10] J. G. Wang, D. X. Wang, and M. Reiser, Nucl. Instrum. Methods Phys. Res., Sect. A **316**, 112 (1992).
[11] D. X. Wang, J. G. Wang, D. Kehne, and M. Reiser, Appl. Phys. Lett. **62**, 3232 (1993).
[12] J. G. Wang, D. X. Wang, and M. Reiser, Phys. Rev. Lett. **71**, 1836–1839 (1993).
[13] D. Kehne, K. Low, M. Reiser, T. Shea, C. R. Chang, and Y. Chen, Nucl. Instrum. Methods Phys. Res., Sect. A **278**, 194–197 (1989).
[14] A. Hofmann, CERN Report No. 77-13 (unpublished), p. 139.
[15] W. C. Hahn, Gen. Elec. Rev. **42**, 258 (1939).
[16] S. Ramo, Phys. Rev. **56**, 276 (1939).
[17] A. W. Trivelpiece and R. W. Gould, J. Appl. Phys. **30**, 1784 (1959).
[18] L. Smith, HIFAR-Note-98, 1986 (unpublished).

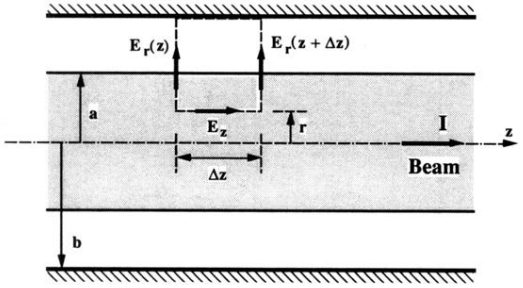

FIG. 8. Configuration to derive theoretical formula for the g factor.